05

The manifestation of surface and size effects in the magnetic properties of ε-Fe$_2$O$_3$ nanoparticles. (Brief overview)

© D.A. Balaev[1], A.A. Dubrovskiy[1], Yu.V. Knyazev[1], S.V. Semenov[1], V.L. Kirillov[2], O.N. Martyanov[2]

[1] Kirensky Institute of Physics, Federal Research Center KSC SB, Russian Academy of Sciences,
Krasnoyarsk, Russia
[2] Boreskov Institute of Catalysis, Siberian Branch of RAS,
Novosibirsk, Russia
E-mail: dabalaev@iph.krasn.ru

Polymorphic modification of iron oxide, known as ε-Fe$_2$O$_3$, exists only in the form of nanoparticles with characteristic sizes up to several tens of nanometers. Particles of these sizes exhibit a large coercive force, about 20 kOe at room temperature. In the temperature range of $80-150$ K, a magnetic transition occurs in ε-Fe$_2$O$_3$, accompanied by a sharp decrease in the coercive force. At the same time, there are significant differences in the magnetic behavior of „large" (~ 20 nm) particles and ultra-small particles (up to 6 nm). A number of experimental facts indicate the manifestation of size effects that lead to a change in the magnetic structure in particles of these sizes. In addition, a surface effect is also manifested for such particles — a significant contribution to the magnetic behavior is governed by surface magnetic anisotropy. In this paper, a brief review of the manifestation of these size and surface effects in the magnetic properties of ε-Fe$_2$O$_3$ nanoparticles is carried out.

Keywords: iron oxide ε-Fe$_2$O$_3$, nanoparticles, size effect, surface magnetic anisotropy.

DOI: 10.21883/PSS.2023.06.56105.12H

1. Introduction

It is now known that trivalent iron oxide Fe$_2$O$_3$ can exist in five polymorphic structural modifications, designated as α, β, γ, ε and ζ. The modifications α and γ, referred to as hematite and maghemite respectively, are the best known and most studied, largely due to the prevalence of these minerals in nature. Other polymorphs are quite rare, and exist only in nanoscale [1,2] form. The newly discovered ζ-Fe$_2$O$_3$ phase is synthesized at high pressure from β-Fe$_2$O$_3$ [2]. Among the less studied iron oxide polymorphs, the most interesting in terms of magnetic properties, and their practical applications, is ε-Fe$_2$O$_3$.

The first mention of the modification ε-Fe$_2$O$_3$ dates back to the 30s [3]. However, reliable identification of the crystal structure ε-Fe$_2$O$_3$ was only made at the end of the 20th century [4]. In Fe$_2$O$_3$ materials in powder form, polymorph ε-Fe$_2$O$_3$ is obtained as nanoparticles up to ~ 30 nm [5,6], or as nanowires with characteristic linear dimensions up to ~ 100 nm [7,8]. There papers are on ε-Fe$_2$O$_3$ nanoparticles as thin films on various substrates [9–11], and papers studying ε-Fe$_2$O$_3$ in borate glasses [12–14]. Recently, the ε-Fe$_2$O$_3$ phase has been found as a dendritic structure in geological rock [15], in the glaze of ancient Chinese porcelain [16] and in the paint of Japanese traditional vase [17]. In these cases, polymorph ε-Fe$_2$O$_3$ was detected in the presence of silicon dioxide; the presence of SiO$_2$ is a necessary factor to produce ε-Fe$_2$O$_3$ nanoparticles in various techniques.

The most important property of ε-Fe$_2$O$_3$ for practical applications is the large coercive force, reaching ~ 20 kOe at room temperature for particle sizes ~ 20 nm [18–20]. In addition, ε-Fe$_2$O$_3$ nanoparticles effectively absorb electromagnetic radiation in the centimeter wave range [1,21,22] (natural magnetic resonance). In this case, it is possible to control the coercive force and the resonance absorption field by varying the particle size and partial iron substitution [21]. The above opens up a wide range of practical applications ε-Fe$_2$O$_3$, emerging when scaling up preparation techniques to large quantities of material and developing high-fill materials ε-Fe$_2$O$_3$. Applications in practical applications in the near future could vary — from highly coercive permanent magnets and materials that absorb electromagnetic radiation to storage media [23].

The impossibility of ε-Fe$_2$O$_3$ as a bulk crystal is due to the low surface energy characteristic of a large structure [1,7]. Therefore, the possibility of realizing ε-Fe$_2$O$_3$ only in the nanoscale can already be considered a surface effect. However, apart from this „thermodynamic surface effect", nanoscale magnetic particles ε-Fe$_2$O$_3$ should also exhibit effects inherent to all magnetic nanoparticles [24]. The implication here is that particles smaller than 30 nm are magnetically single-domain and can exhibit superparamagnetic (SPM) behavior, with the contribution of surface magnetic anisotropy to SPM blocking processes likely to be significant. It is also likely that particle size affects the temperature of magnetic transitions of the order-non-order type, or the transition from one type of magnetic
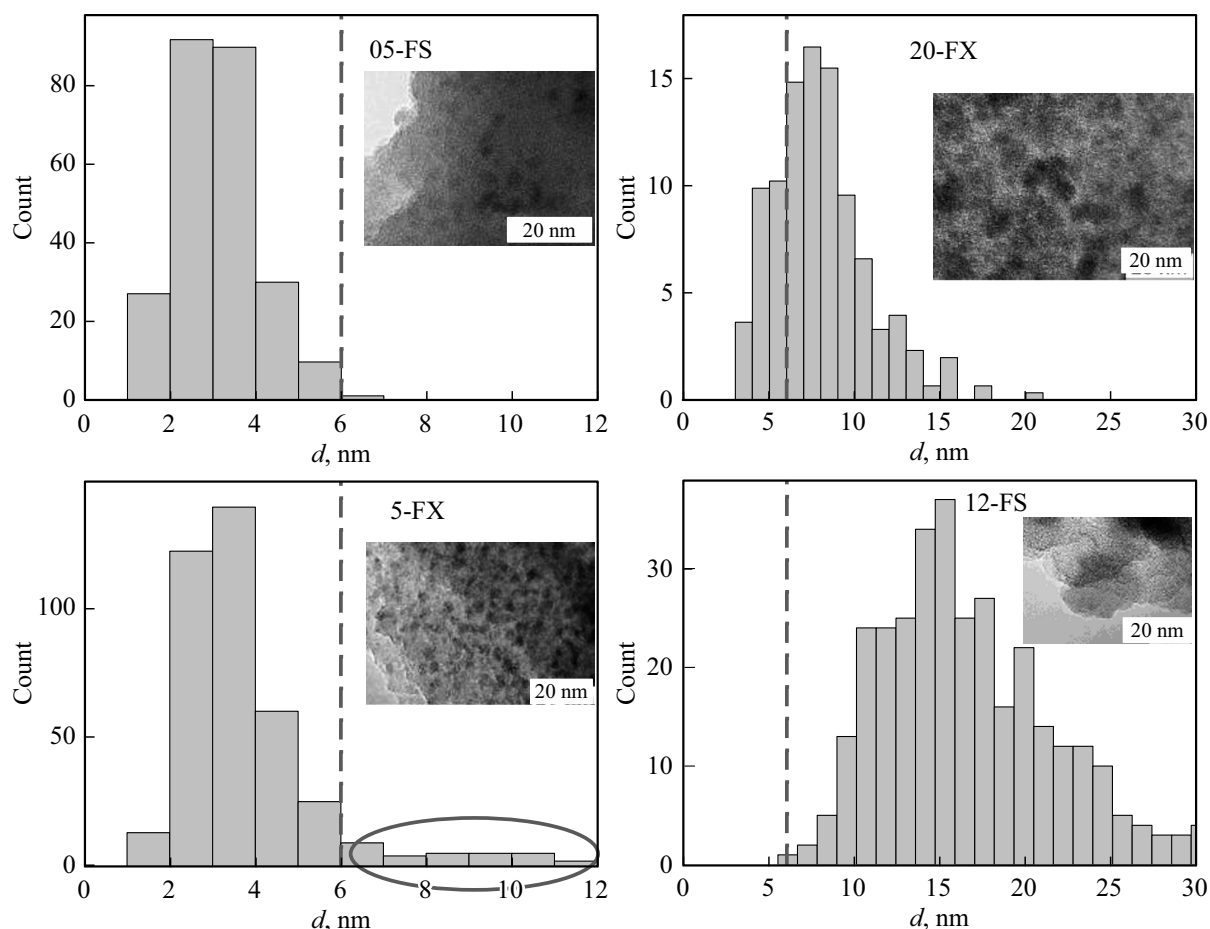
Figure 1. Particle size distributions of some samples of series x-FS and x-FX. Typical HR TEM microphotographs are shown in the histogram field. The oval in the histogram below left illustrates the difference in distributions for samples 05-FS and 5-FX.

structure to another. Clear examples of this size effect with decreasing particle size are the lowering of the transition temperature from the magnetic-ordered to the paramagnetic state [25–27], the decreasing values of the Morin and Verwey characteristic temperatures for hematite [25–27] and magnetite [28–30], respectively. At a certain critical particle size, the above Morin and Verwey transitions are not observed.

In structure ε-Fe_2O_3, the iron atoms occupy four non-equivalent positions, which makes it possible to realize a rather complex magnetic structure. It is now generally accepted that in the temperature range of $150-500$ K in ε-Fe_2O_3 a ferrimagnetic collinear structure [1] is realized, but in the temperature range of 150 to 80 K in ε-Fe_2O_3, a magnetic transition occurs leading to a drastic change in the magnetic characteristics [19–21]. Therefore, similar to other iron oxides and magnetic materials, for ε-Fe_2O_3, it is essential to understand the influence of particle size on the presence of the specified magnetic transition. Also important is the way other surface effects are manifested. The present paper is a brief review of the magnetic properties of ultra-small particles ε-Fe_2O_3, which basically summarizes the data obtained by the group of authors of

this paper. Here, the term „ultra-small" refers to sizes $\sim 3-8$ nm, while „large sizes" — correspond to particles on the order of $20-30$ nm.

2. Techniques for producing ultra-small particles ε-Fe_2O_3

In Fe_2O_3 early noughties of this century the collaborators of G.K. Boreskov Institute of Catalysis of SB RAS proposed two fairly simple methods of obtaining ultrafine particles ε-Fe_2O_3, which allowed to obtain samples that do not contain polymorphs of other iron oxides. In the first method, the silica gel is impregnated with Fe(II) sulfates, held at $110°C$ and annealed at $900°C$ [31,32]. The samples are ε-Fe_2O_3 nanoparticles immobilized in silica gel pores. Typical results from high-resolution transmission electron microscopy (HR TEM) are shown in Fig. 1. In this method, the average $\langle d \rangle$ and maximum d_{max} particle sizes are determined by the amount of initial Fe(II) sulfate and the resulting iron concentration (see Fig. 1). Up to a concentration Fe (x) 12 wt.%, the samples are practically single-phase — the amount of „the parasitic" phase of

hematite does not exceed 4 wt% (of total Fe_2O_3) with total iron content in the sample of 12.5 wt.%, and at Fe 3.4 wt.%, no other iron oxide phase other than ε-Fe_2O_3 [33] is observed in the samples. This sample series is further designated as x-FS.

The second technique for the preparation of ε-Fe_2O_3 involves the incorporation of Fe(II) salts into SiO_2 hydrogel by diffusion exchange followed by drying and annealing [34]. The samples obtained by this method are low-density bulk composites which contain ε-Fe_2O_3 nanoparticles in SiO_2 xerogel pores. This sample series is further designated as x-FX. Fig. 1 shows typical HR TEM results and size distribution for samples of series x-FX. At x to ≈ 24 wt.%, no parasitic hematite phase was detected.

The presence of iron oxide phase ε-Fe_2O_3 (above 95%) for both series samples was confirmed by X-ray diffraction analysis (spatial group $Pna21$) and Mössbauer spectra [33,34] analysis.

3. Coercive force: dependence on particle size and temperature

Fig. 2 shows typical magnetic hysteresis loops for selected FS and FX series samples. Logically, the coercive force is greater for larger particles because, even particles of size 30 nm are in a single-domain state [7]. For single-domain particles, thermal fluctuations begin to play a significant role, which has a well-known name — the superparamagnetizm effect. In SPM state, the magnetization curve is modelled by a Langevin function and the data in Fig. 2 for the sample 05-FS has been described by a Langevin function with the particle size distribution [35]. The particle size distribution also affects the value of the experimentally determined coercive force, since magnetization is — integral effect. The presence of small SPM particles in the sample leads to a specific type of hysteresis loop — the so-called „wasp-shaped" — a narrowing of the loop in area $M \sim 0$. This is shown by $M(H)$ dependencies for samples 12-FS and 20-FX. Therefore, the value of H_C for an ensemble of particles may not correspond to the coercive force of average sized particles. The authors [36] obtained the $H_C(d)$ dependence for a large number of samples with different particle sizes ε-Fe_2O_3, these data are shown in Fig. 3. In the same figure, we also show data for series samples x-FS and x-FX. Some discrepancy between values H_C of sample of series x-FS (at $x = 12$ and 16 vol.%) according to paper [36] is due to influence of particles of smalle sizes.

In the SPM state, the direction of magnetic moment of a single-domain particle changes with frequency $\sim 1/\tau$, with the freezing temperature „of the magnetic moment" in the energy potential $K \cdot V$ (V — particle volume) or, SPM-blocking temperature T_B determined by the Néel–Brown relation:

$$T_B = K \cdot V / \ln(\tau/\tau_0). \qquad (1)$$

In expression (1) τ_0 — the characteristic relaxation time of the particle's magnetic moment (τ_0 — is within
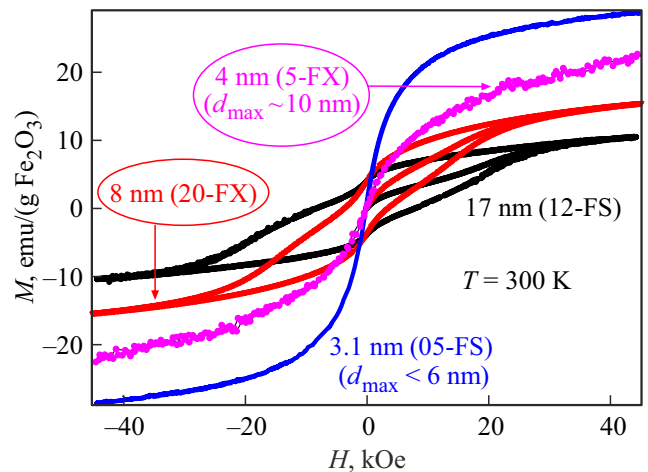

Figure 2. Dependencies $M(H)$ at $T = 300$ K of the selected samples; the average and maximum (for two samples) particle sizes are indicated.
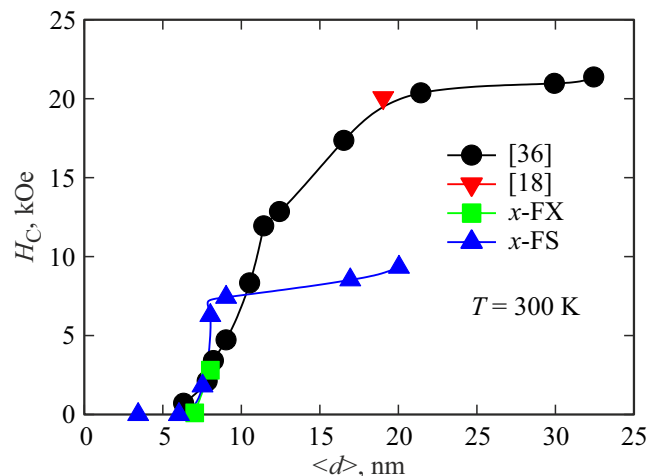

Figure 3. Coercive force dependence on average particle size ε-Fe_2O_3 at $T = 300$ K according to papers [36,18] and for samples of series x-FS and x-FX.

$10^{-9}-10^{-13}$ s). If τ is the same as the characteristic time of the measuring technique τ_m, then ratio (1) predicts the dependence of T_B on V. Also, from expression (1) the critical volume (and hence the critical particle size) for the so-called superparamagnetic limit at a certain temperature can be found. For quasi-static magnetometry $\tau_m = \tau_{m\,VSM} \sim 1-100$ s, therefore if $T \approx T_B$, the superparamagnetic limit state is realized, and there will be no hysteresis on the magnetization curve (H_C will be zero). From the aggregate data in Fig. 3, it can be concluded that the critical size value for ε-Fe_2O_3 at room temperature is of the order of 6−7 nm.

Let us turn to the temperature dependence of the coercive force of different size particles. Fig. 4 shows the $H_C(T)$ dependences for particles with an average size of 20 nm (according to [18]), 8 nm (sample 20-FX), 4 nm (sample
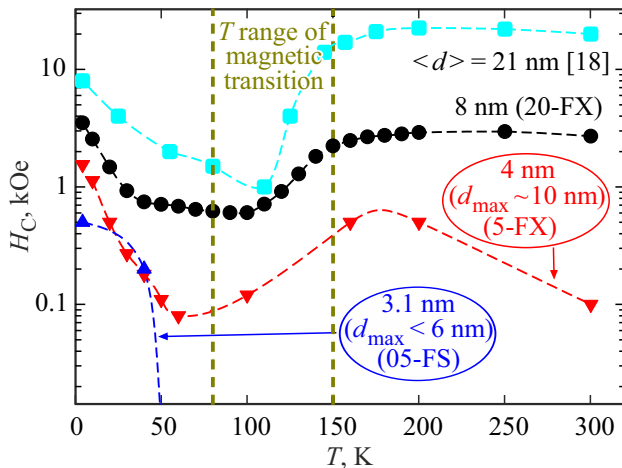
Figure 4. Temperature dependences of coercive force $H_C(T)$ for nanoparticle samples ε-Fe$_2$O$_3$ of indicated sizes (data of paper [18] and samples of series x-FS and x-FX). The vertical dashed lines indicate the temperature range in which the magnetic transition occurs in ε-Fe$_2$O$_3$.

5-FX) and 3.1 nm (sample 05-FS). As can be seen, for most of the data in Fig. 4, there is a non-monotonic behavior of $H_C(T)$, namely, with decreasing temperature, below 150 K a sharp (order of magnitude) decrease in the coercive force takes place. This is due to the magnetic transition in ε-Fe$_2$O$_3$, mentioned above (in the Introduction), occurring in the interval $\sim 80-150$ K [1,7,18–20]. This magnetic transition is a „calling card" ε-Fe$_2$O$_3$, in the specified temperature range a distortion of the crystal structure [20] occurs, changing a number of parameters that show a relationship to the magnetic structure [37–41]. As a result, the incommensurate structure of the spiral type [1,20,41,42] is assumed to be formed in the low temperature area, although this question remains largely open. In this review, we focus on the presence of this transition in ultra-small particles, see the following section.

4. Magnetic transition in ε-Fe$_2$O$_3$ particles and the superparamagnetic state

As can be seen from Fig. 4, for the sample 05-FS, the coercive force becomes negligibly small above 50 K, and its increase after the magnetic transition (in interval $\sim 80-150$ K) with increasing temperature is absent. Comparing the size distributions of samples 05-FS and 5-FX, one can notice that in the sample 5-FX, there is a small number of particles from 6 to 10 nm (see Fig. 1), from which we can conclude that exactly the particles of this size contribute to the non-monotonic behavior $H_C(T)$ of sample 5-FX.

Apart from the SPM state criterion, such as $H_C = 0$, the most commonly used method for determining the blocking temperature is to study the temperature dependence of magnetization under zero external field cooling (ZFC)

and cooling in a magnetic field of some magnitude (FC). $M(T)_{ZFC}$ dependence shows a maximum in the vicinity of the temperature T_B, and the divergence of the $M(T)_{ZFC}$ dependence from the $M(T)_{FC}$ dependence at some temperature T_{irr} (usually $T_{irr} > T_B$) corresponds to the blocking of the largest particle size. In the case of nanoparticles ε-Fe$_2$O$_3$, it is necessary to distinguish the blocking of particle magnetic moments from the manifestation in the magnetization behavior of the magnetic transition in the interval $\sim 80-150$ K.

Fig. 5 shows $M(T)$ dependencies for the samples of series x-FS (a) and x-FX (b). In this figure, the temperature intervals of the magnetic transition (characteristic for ε-Fe$_2$O$_3$) are marked (vertical dashed lines) and the average particle size of the samples is indicated. If we refer to the data of Fig. 5, a, we can conclude that for samples 3-FS, 7-FS and 12-FS, anomalies in the behavior of magnetization are observed in the interval corresponding to the magnetic transition. However, for the sample 05-FS, the dependence $M(T)$ behaves monotonically in the specified temperature range (also monotonically at higher temperatures). At the
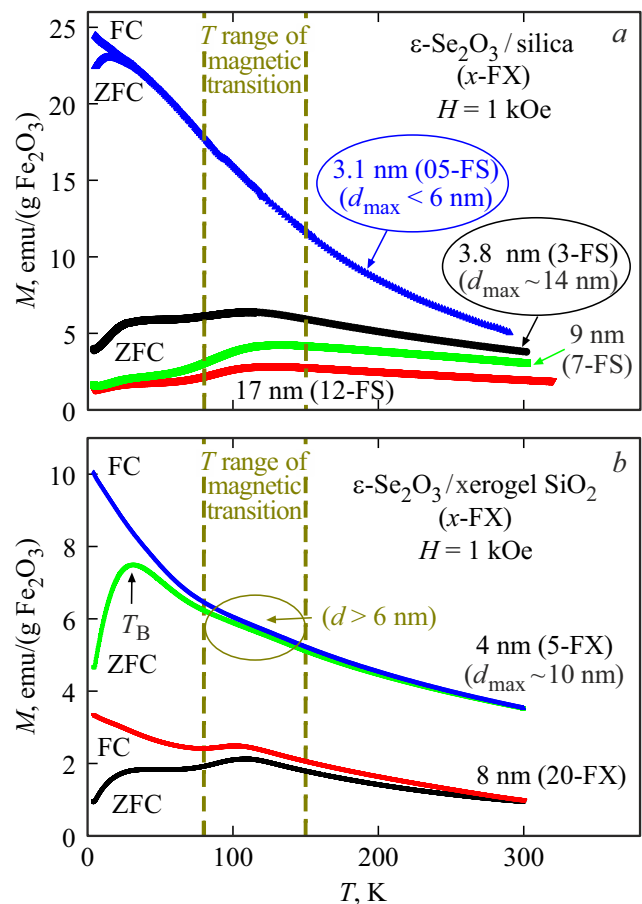

Figure 5. Temperature dependences of magnetization in $H = 1$ kOe field (ZFC and FC modes indicated) of the x-FS (a) and samples of series x-FX (b). The vertical dashed lines indicate the temperature range in which the magnetic transition occurs in „large" particles ε-Fe$_2$O$_3$.
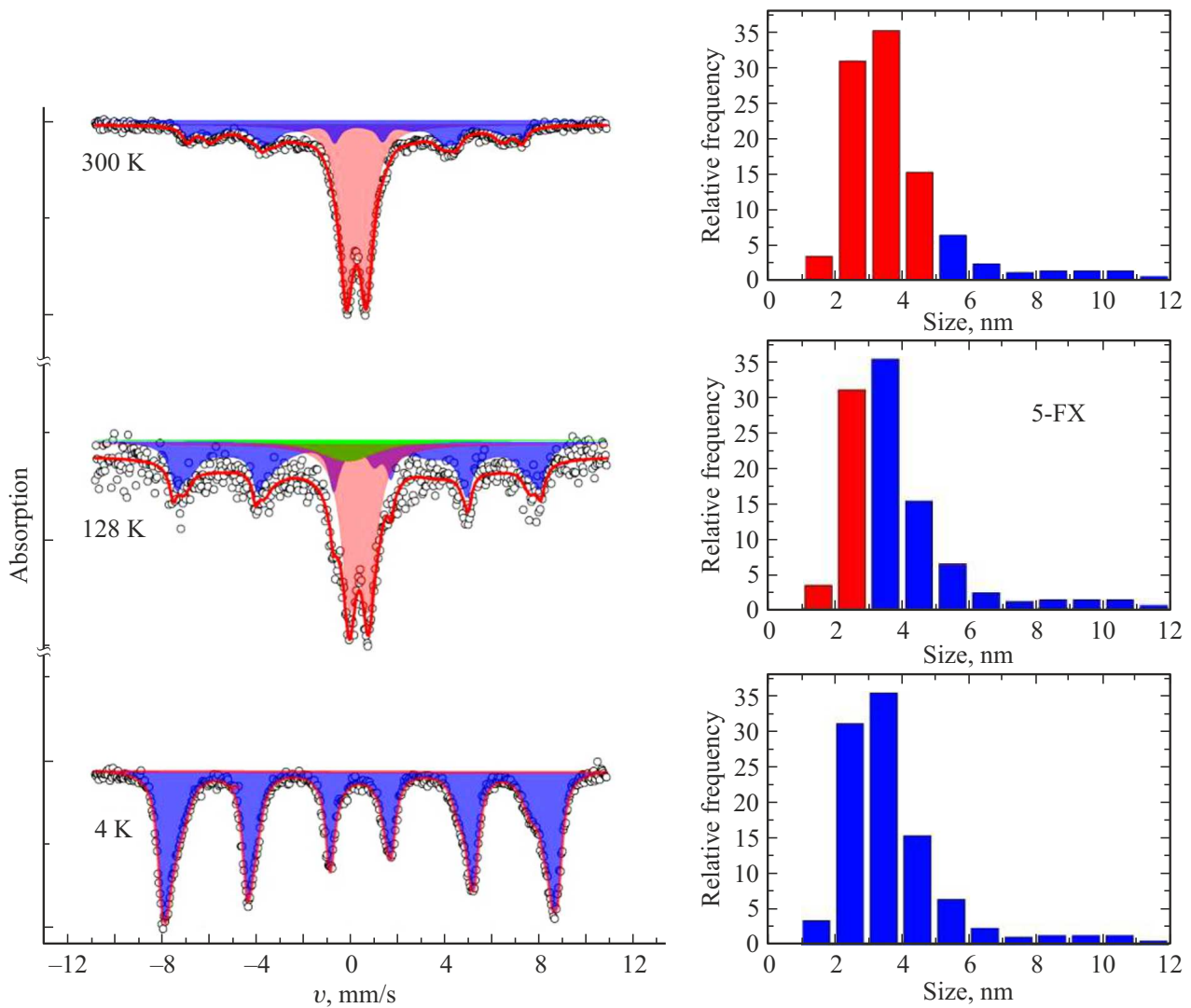
Figure 6. Mössbauer spectra of the sample 5-FX at the indicated temperatures (left). Solid lines — results of analysis of the spectra (partial components — sextet, doublet and single relaxation line are color coded, see text in section 5). To the right: particle size distribution, showing which particles (at a given temperature) are in the SPM state (red) and which are in the blocked state (blue).

same time, in the low temperature area, the dependences $M(T)_{ZFC}$ and $M(T)_{FC}$ for this sample, exhibit behavior typical of the transition processes from the SPM state to the blocked state (presence of a maximum in the dependence $M(T)_{ZFC}$). For the sample 05-FS the maximum size does not exceed 6 nm (see Fig. 1), hence, it can be concluded that in particles ε-Fe$_2$O$_3$ of such ultra small size there is no magnetic transition.

Analysis of the data in Fig. 5, b confirms the above. In sample 20-FX the vast majority of particles are larger than 6 nm (Fig. 1) and the magnetic transition in the interval $\sim 80-150$ K is clearly visible. In the sample 5-FX the fraction of particles larger than 6 nm is small (Fig. 1). And, the change (though rather weak) in the temperature dependence of magnetization in the interval $\sim 80-150$ K (marked with an oval) seen in Fig. 5, b is due to these particles ($d > 6$ nm). At the same time, for the

SPM-blocking processes (maximum $M(T)_{ZFC}$ dependence) for the 5-FX sample in the low temperature area are „responsible" for particles smaller than 6 nm.

The data for the sample 3-FS (Fig. 5, a) do not contradict our reasoning. Although the average particle size of the 3-FS sample is small ($\langle d \rangle \approx 3.8$ nm), the distribution is quite broad [42] ($d_{max} \sim 14$ nm) and the larger particles exhibit a magnetic transition ($\sim 80-150$ K). The SPM blocking of small particles appears on the $M(T)_{ZFC}$ dependence as a „plateau" in the low temperature area.

Thus, a comparative analysis of the temperature dependence of the magnetization of the x-FS and x-FX series samples showed that the magnetic transition in ε-Fe$_2$O$_3$ is absent for particles smaller than 6 nm. This can be considered a manifestation of a size effect similar to the decrease of the Morin characteristic temperatures for hematite [25–27] and Verwey for magnetite [28–30] (and the complete

absence of these transitions) with decreasing particle size. For ε-Fe$_2$O$_3$, particles smaller than 6 nm SPM magnetic moment blocking processes are observed.

5. Superparamagnetic blocking in different techniques and magnetic anisotropy constant for ε-Fe$_2$O$_3$ particles

The data presented in the previous section allow to derive $M(T)_{\text{ZFC}}$ and $M(T)_{\text{FC}}$ temperatures from a joint analysis of dependences T_B and T_{irr} (Fig. 5) and particle size distributions (Fig. 1) (T_{irr}, temperature is only observed for sample 05-FS and corresponds to the largest particle size lock — 6 nm, see Fig. 5, a). However, in addition to quasi-static magnetization, other techniques with different characteristic measurement times τ_{m} are possible. For Mössbauer spectroscopy the value of $\tau_{\text{m}} = \tau_{\text{m MS}}$ is $\sim 10^{-8}$ s [43], hence for the same particle size, the blocking temperatures for magnetization and Mössbauer effect, according to expression (1), will differ several times (the multiplier $\sim \ln(\tau_{\text{m VSM}}/\tau_{\text{m MS}})$). For nanoparticles in the blocked state, the Mössbauer spectrum is a sextet (with parameters close to those of the bulk material), while the unblocked state of the particles' magnetic moments is characterized by a doublet [44–46]. In its parameters, the SPM doublet is similar to the paramagnetic behavior of iron nuclei spins, but one must realize that in the SPM state, the magnetic order inside the particle remains, and the magnetic moment of the particle changes its direction with a frequency greater than $1/\tau_{\text{m MS}}$.

Fig. 6 (left) shows the Mössbauer spectra of the sample 5-FX at different temperatures. For a temperature of 4 K, the magnetic moments of the particles are blocked, and the spectrum is a sextet. As the temperature rises, a doublet appears in the spectrum, the proportion of which increases with temperature. A single broad line in the spectra, which corresponds to those particles for which the condition $\tau_{\text{m MS}} \sim \tau_0$ was fulfilled, was also detected. Processing the spectra [47] allows us to distinguish the ratios of the magnetically split (sextet) A_{sex} and SPM component A_{dou} spectra (in Fig. 6 highlighted in the corresponding color). Obviously, $A_{\text{sex}}/A_{\text{dou}}$ is approximately equal to the ratio of the total volumes $V_{\text{bloked}}/V_{\text{SPM}}$ of particles in the blocked (V_{bloked}) and unblocked (V_{SPM}) states. This allows one to determine the part of the size distribution, in which the magnetic moments of the particles are in the SPM state (the other part — in the blocked state) for each temperature, which is graphically illustrated (highlighted) in Fig. 6 (to the right).

Note also that in ferromagnetic resonance, the value $\tau_{\text{m}} = \tau_{\text{m FMR}} \sim 1/f$ (f — microwave frequency). In paper [48], based on a comparison of spectra ($f = 9.4$ GHz) of samples of series x-FS, and simulated spectra, it was found that the SPM blocking temperature of particles less than ~ 2 nm is $\sim 110-130$ K.
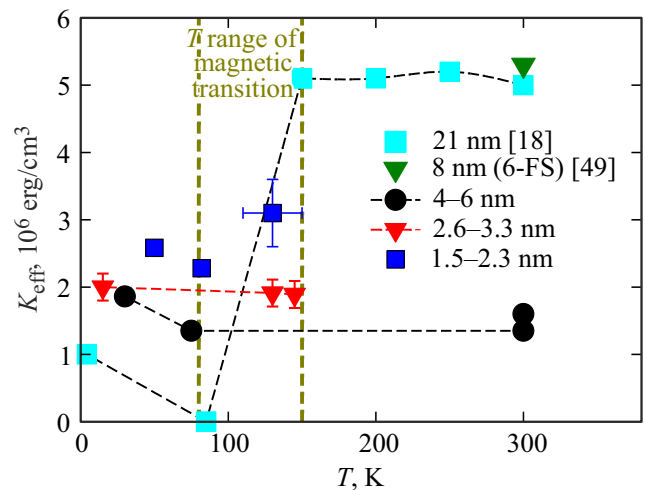
Figure 7. Temperature dependences of the effective magnetic anisotropy constant K_{eff} of ε-Fe$_2$O$_3$ nanoparticles of different sizes (indicated in the legend); for size 20 nm data from [18] are used. The vertical dashed lines indicate the temperature range in which the magnetic transition occurs in „large" particles.

For known values of particle size and SPM blocking temperature, using expression (1), it is possible to obtain the value of the magnetic anisotropy constant K. Note, that expression (1) is only valid for magnetically non-interacting particles but the resulting estimates of K have been made for porous samples with low volume concentration ε-Fe$_2$O$_3$, so magnetic inter-particle interactions can be neglected. In addition, here and hereafter, instead of the designation K for the magnetic anisotropy constant, we introduce the designation K_{eff}, referring to effects due to the contribution of surface magnetic anisotropy — in this case, especially for small particles, it makes sense to speak of an effective magnetic anisotropy constant K_{eff}.

The data obtained from the SPM state transition temperature analysis — K_{eff} and T values for the different techniques, are shown in Fig. 7. In this figure, the data for small particles are grouped by size range (4–6 nm, 2.6–3.3 nm, 1.5–2.3 nm) of particles and are combined by symbol type (as indicated in the legend). For the sample 6-FS ($\langle d \rangle \approx 8$ nm) the value K_{eff} was obtained in [49] from analysis of the coercive force dependence on the remagnetization rate. Fig. 7 also shows the data obtained in [18]. In the aforementioned paper, the magnetization curve approximation to saturation method was used to derive a magnetic anisotropy constant equal to $5 \cdot 10^6$ erg/cm^3 at $T = 300$ K. In addition, the anisotropy constant at temperatures of 80 K and 4 K has been estimated in [18]. We calculated the K_{eff} values at temperatures of 250, 200 and 150 K from the H_C and M_S (saturation magnetization) [18] using the ratio $H_C \approx 2K/M_S$.

From Fig. 7, one can see a sharp decrease (according to [18] to $\sim 10^2$ erg/cm^3) of the magnetic anisotropy constant of „large" particles (20 nm) with decreasing temperature from 150 K to 80 K, which reflects the change

in magnetic structure during the magnetic transition. As the temperature further decreases, the value K_{eff} slightly increases. However, for particle sizes up to 6 nm the data do not show a similar trend in temperature evolution: values K_{eff} take intermediate values between the values K_{eff} of „large" particles at 300 and 4 K. In this case, we should already consider the dependence K_{eff} on particle size, which we have done in the next Section.

6. Exposure to surface magnetic anisotropy contribution

One striking manifestation of surface effects in the magnetic properties of small particles is the contribution of surface magnetic anisotropy. This contribution is caused by the large proportion of atoms in nonstoichiometric („not full") surroundings on the particle surface [50,51]. The corresponding additional magnetic anisotropy energy can be written as $K_S \cdot S$, where K_S — magnetic anisotropy constant, S — particle surface area [52]. By combining the bulk anisotropy energy $K_V \cdot V$ (K_V — the bulk magnetocrystalline anisotropy constant) and the surface anisotropy constant $K_S \cdot S$, the expression $K_{eff} \cdot V = (K_V + 6K_S/d) \cdot V$ [53] can be found. Here K_{eff} — the effective magnetic anisotropy constant (it corresponds to the constant K_{eff} introduced in section 5) and its relation to the values K_V and K_S is expressed as follows:

$$K_{eff} = K_V + 6K_S/d. \tag{2}$$

Expression (2) predicts an increase in the effective anisotropy constant with decreasing particle size. A number of papers on various nanoparticle systems [53–62] have yielded results indicating that the contribution of surface magnetic anisotropy can be considered, according to expression (2).

Fig. 8 shows values K_{eff} for ε-Fe$_2$O$_3$ (see Section 5) as a function of the inverse particle size $1/d$. In this figure, the data for particles smaller than 6 nm for each particular technique are grouped with the same symbols (see legend and caption of Fig. 8). It can be seen that, in the coordinates used, these data fit well on a straight line, according to expression (2). This indicates that the increase in K_{eff} with decreasing particle size is indeed due to an increase in the contribution of surface magnetic anisotropy. The straight line in Fig. 8 is plotted at $K_V = 7.2 \cdot 10^5$ erg/cm^3, $K_S = 0.06$ erg/cm^2; the relative error of these values can be given as $5-7\%$.

It can also be seen from Fig. 8, that the value of K_{eff} at $T = 4$ K for 20 nm particles also falls into the obtained dependence of expression (2). At the same time, values K_{eff} at $T = 300$ K for large particles are much larger than K_{eff} values for particles smaller than 6 nm, and K_{eff} at 80 K (for size 20 nm) is much smaller than K_{eff} for small particles. The collinear magnetic structure in ε-Fe$_2$O$_3$ is realized in the temperature range from 150 to 500 K [63–65]. In the low temperature area, the magnetic structure stabilizes
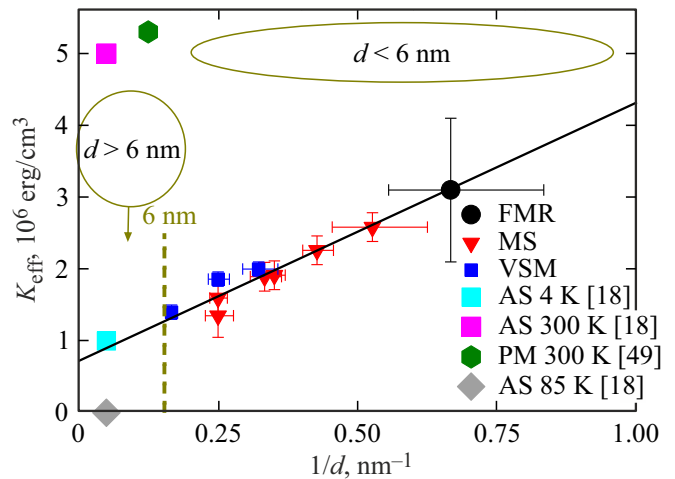

Figure 8. Dependence of the effective magnetic anisotropy constant K_{eff} on the inverse particle size ($1/d$). Designations in the legend: VSM — quasi-static magnetic measurements, MS — Mössbauer spectroscopy, FMR — ferromagnetic resonance, AS — approaching saturation magnetization, PM — pulse remagnetization. The data from the papers mentioned in the legend are also used. The vertical dashed line corresponds to $d = 6$ nm.

not immediately after the transition $(80-150\,\text{K})$, and this is indirectly confirmed by the behavior of a number of experimentally determined parameters [20,37–41,66]. The above experimental facts can be attributed to the fact that the magnetic structure in small particles is close to the magnetic structure of „large" particles at 4 K. Indeed, it can be stated that the values K_V for „large" particles at 4 K and small particles (already for the whole temperature range) coincide.

Note also, that the contribution of the surface magnetic anisotropy energy can be quite simply estimated from Fig. 8. In fact, it is the difference between the value of K_{eff} (ordinate) and K_V (point where the straight line intersects the ordinate axis). For particles of size 4 nm $(1/d = 0.25\,\text{nm}^{-1})$, the surface magnetic anisotropy energy is approximately the same as the value $K_V \cdot V$. For smaller particles, the contribution from surface magnetic anisotropy dominates. For a particle size of 20 nm this contribution at $T = 4$ K is about 20%. However, at 300 K, when $K_{eff} = 5 \cdot 10^6$ erg/cm^3, the contribution from surface anisotropy will only be about 4%. Note, that the value $K_S \approx 0.06$ erg/cm^2 given here is quite close to the value $K_S \approx 0.1$ erg/cm^2 obtained in [49] from the analysis of pulse remagnetization processes of particles ε-Fe$_2$O$_3$ of size 8 nm.

7. Conclusion

To summarize the experiments described in this short review related to the manifestation of size and surface effects in ε-Fe$_2$O$_3$, the following can be said. The magnetic transition between $80-150$ K, which is the „calling card" ε-Fe$_2$O$_3$, is not observed for particles less than

6 nm. Particles of these sizes exhibit transitions from the superparamagnetic to the blocked state, which is captured by techniques with different characteristic measurement times (magnetometry, Mössbauer spectroscopy). Surface magnetic anisotropy begins to play a significant role in the magnetic properties of such particles. The data made it possible, within the framework of the known $K_{\text{eff}} = K_V + 6 \cdot K_S/d$ relation, to separate the contributions of the bulk and surface magnetic anisotropy energies and to obtain the values K_V and K_S. K_S ($0.06 \, \text{erg/cm}^2$) is typical of oxide materials. The value K_V ($7.2 \cdot 10^5 \, \text{erg/cm}^3$) for small particles was much lower than the magnetic anisotropy constant of „large" particles ε-Fe_2O_3 at room temperature ($5 \cdot 10^6 \, \text{erg/cm}^3$). However, the value K_V obtained is in good agreement with that for „large" particles ε-Fe_2O_3 at low temperature. The latter indirectly indicates that the magnetic structure of small particles is similar to the low-temperature magnetic state „large" particles ε-Fe_2O_3. The superparamagnetic limit (for magnetometry) at room temperature for ε-Fe_2O_3 is about 7 nm. And this size are „at the edge" of the transition from the „quasi-bulk" state („large" particles) ε-Fe_2O_3 to the magnetic state of ultrafine particles described above.

Conflict of interest

The authors declare that they have no conflict of interest.

References

[1] J. Tuček, R. Zbořil, A. Namai, S. Ohkoshi. Chem. Mater. **22**, 6483 (2010).

[2] J. Tuček, L. Machala, S. Ono, A. Namai, M. Yoshikiyo, K. Imoto, H. Tokoro, S. Ohkoshi, R. Zbořil. Sci. Rep. **5**, 15091 (2015).

[3] H. Forrestier, G.C. Guiot-Guillain, C.R. Acad. Science (Paris) 199, 720 (1934).

[4] E. Tronc, N. Chaneac, J.P. Jolivet. J. Solid State Chem. **139**, 93 (1998).

[5] V.N. Nikolic, M. Tadic, M. Panjan, L. Kopanja, N. Cvjeticanin, V. Spasojevic. Ceram. Int. **43**, 3147 (2017).

[6] V.N. Nikolic, V. Spasojevic, M. Panjan, L. Kopanja, A. Mrakovic, M. Tadic. Ceram. Int. **43**, 7497 (2017).

[7] S. Ohkoshi, H. Tokoro. Bull. Chem. Soc. Jpn. **86**, 897907 (2013).

[8] A.I. Dmitriev, O.V. Koplak, A. Namai, H. Tokoro, S. Ohkoshi, R.B. Morgunov. FTT **56**, 1735 (2014). (in Russian).

[9] M. Gich, J. Gazquez, A. Roig, A. Crespi, J. Fontcuberta, J.C. Idrobo, S.J. Pennycook, M. Varela, V. Skumryev, M. Varela. Appl. Phys. Lett. **96**, 112508 (2010).

[10] S.M. Suturin, A.M. Korovin, A.A. Sitnikova, D.A. Kirilenko, M.P. Volkov, P.A. Dvortsova, V.A. Ukleev, M. Tabuchi, N.S. Sokolov. Sci. Technol. Adv. Mater. **22**, 86 (2021).

[11] A. Philip, J.-P. Niemela, G.C. Tewari, B. Putz, T.E.J. Edwards, M. Itoh, I. Utke, M. Karppinen. ACS Appl. Mater. Interfaces **12**, 21912 (2020).

[12] Edelman, J. Kliava, O. Ivanova, R. Ivantsov, D. Velikanov, V. Zaikovskii, E. Petrakovskaja, Y. Zubavichus, S. Stepanov. J. Non-Crystalline Solids **506**, 68 (2019).

[13] O.S. Ivanova, R.D. Ivantsov, I.S. Edelman, E.A. Petrakovskaja, D.A. Velikanovb, Y.V. Zubavichus, V.I. Zaikovskii, S.A.Stepanov. J. Magn. Magn. Mater. **401**, 880 (2016).

[14] R.M. Eremina, I.V. Yatsyk, A.V. Shestakov, I.I. Fazlizhanov, T.P. Gavrilova, F.O. Milovich, A.L. Zinnatullin, F.G. Vagizov, I.F. Gilmutdinov, P.S. Shirshnev, D.I. Sobolev, N.V. Nikonorov. J. Phys. Chem. Solids **133**, 7 (2019).

[15] H. Xu, S. lee, H. Xu. Am. Mineralog. **102**, 711 (2017).

[16] L. Wang, Y. Wang, M. Zhang, Q. Li, J. Wu, Z. Liu, L. Li, X. Wie. Anal. Chem. **91**, 13054 (2019).

[17] Y. Kusano, H. Nakata, Z. Peng, R.S.S. Maki, T. Ogawa, M. Fukuhara. ACS Appl. Mater. Interfaces **13**, 38491 (2021).

[18] M. Gich, A. Roig, C. Frontera, E. Molins, J. Sort, M. Popovici, G. Chouteau, D.M. Marero, J. Nogues. J. Appl. Phys. **98**, 044307 (2005).

[19] M. Kurmoo, J.-L. Rehspringer, A. Hutlova, C. D'Orlans, S. Vilminot, C. Estournes, D. Niznansky. Chem. Mater. **17**, 1106 (2005).

[20] M. Gich, C. Frontera, A. Roig, E. Taboada, E. Molins. Chem. Mater. **18**, 3889 (2006).

[21] S. Ohkoshi, A. Namai, T. Yamaoka, M. Yoshikiyo, K. Imoto, T. Nasu, S. Anan, Y. Umeta, K. Nakagawa, H. Tokoro. Sci. Rep. **6**, 27212 (2016).

[22] E. Gorbachev, M. Soshnikov, M. Wu, L. Alyabyeva, D. Myakishev, E. Kozlyakova, V. Lebedev, E. Anokhin, B. Gorshunov, O. Brylev, P. Kazin, L. Trusov. J. Mater. Chem. C, **9**, 6173 (2021).

[23] S. Ohkoshi, A. Namai, M. Yoshikiyo, K. Imoto, K. Tamazaki, K. Matsuno, O. Inoue, T. Ide, K. Masada, M. Goto, T. Goto, T. Yoshida, T. Miyazaki. Angew. Chem. **128**, 1 (2016).

[24] S. Bedanta, W. Kleemann. J. Phys. D **42**, 013001 (2009).

[25] C. Díaz-Guerra, L. Pérez, J. Piqueras, M.F. Chioncel. J. Appl. Phys. **106**, 104302 (2009).

[26] R.D. Zysler, D. Fiorani, A.M. Testa, L. Suber, E. Agostinelli, M. Godinho. Phys. Rev. B **68**, 212408 (2003).

[27] M. Tadic, D. Markovic, V. Spasojevic, V. Kusigerski, M. Remskar, J. Pirnat, Z. Jaglic. J. Alloys Comp. **441**, 291 (2007).

[28] D. Sarkar, M. Mandal, K. Mandal. J. Appl. Phys. **112**, 064318 (2012).

[29] X.b. Jiang, B.b. Xiao, H. yu Yang, X. y. Gu, H.ch. Sheng, X.h. Zhang. Appl. Phys. Lett. **109**, 203110 (2016).

[30] R.N. Bhowmik, A. Saravanan. J. Appl. Phys. **107**, 053916 (2010).

[31] G.A. Bukhtiyarova, M.A. Shuvaeva, O.A. Bayukov, S.S. Yakushkin, O.N. Martyanov. J. Nanopart. Res. **13**, 5527 (2011).

[32] G.A. Bukhtiyarova, O.N. Martyanov, S.S. Yakushkin, M.A. Shuvaeva, O.A. Bayukov. FTT **52**, *4*, 771 (2010). (in Russian).

[33] S.S. Yakushkin, D.A. Balaev, A.A. Dubrovskiy, S.V. Semenov, K.A. Shaikhutdinov, M.A. Kazakova, G.A. Bukhtiyarova, O.N. Martyanov, O.A. Bayukov. J. Supercond. Nov. Magn. **31**, 1209 (2017).

[34] S.S. Yakushkin, D.A. Balaev, A.A. Dubrovskiy, S.V. Semenov, Yu.V. Knyazev, O.A. Bayukov, V.L. Kirillov, R.D. Ivantsov, I.S. Edelman, O.N. Martyanov. Ceram. Int. **44**, 17852 (2018).

[35] D.A. Balaev, A.A. Dubrovskiy, K.A. Shaykhutdinov, O.A. Bayukov, S.S. Yakushkin, G.A. Bukhtiyarova, O.N. Martyanov. J. Appl. Phys. **114**, 163911 (2013).

[36] S. Ohkoshi, A. Namai, K. Imoto, M. Yoshikiyo, W. Torora, K. Nakagawa, M. Komine, Y. Miyamoto, T. Nasu, S. Oka, H. Tokoro. Sci. Rep. **5**, 14414 (2015).

[37] Y.Ch. Tseng, N.M. Souza-Neto, D. Haskel, M. Gich, C. Frontera, A. Roig, M. van Veenendaal, J. Nogués. Phys. Rev. B **79**, 094404 (2009).

[38] E. Tronc, C. Chanéac, J.P. Jolivet. J. Appl. Phys. **98**, 053901 (2005).

[39] J. Kohout, P. Brázda, K. Závěta, D. Kubániová, T. Kmječ, L. Kubíčková, M. Klementová, E. Šantavá, A. Lančok. J. Appl. Phys. **117**, 17D505 (2015).

[40] Y.V. Knyazev, A.I. Chumakov, A.A. Dubrovsky, S.V. Semenov, S.S. Yakushkin, V.L. Kirillov, O.N. Martyanov, D.A. Balaev. Pis'ma ZhETF, **110**, 614 (2019). (in Russian).

[41] Yu.V. Knyazev, A.I. Chumakov, A.A. Dubrovskiy, S.V. Semenov, I. Sergueev, S.S. Yakushkin, V.L. Kirillov, O.N. Martyanov, D.A. Balaev. Phys. Rev. B **101**, 094408 (2020).

[42] S.S. Yakushkin, A.A. Dubrovskiy, D.A. Balaev, K.A. Shaykhutdinov, G.A. Bukhtiyarova, O.N. Martyanov. J. Appl. Phys. **111** *4*, 044312 (2012).

[43] S. Mørup, D.E. Madsen, C. Fradsen, C.R.H. Bahl, M.F. Hansen. J. Phys.: Condens. Matter **19**, 213202 (2007).

[44] J. Fock, M.F. Hansen, C. Frandsen, S. Mørup. J. Magn. Magn. Mater. **445**, 11 (2018).

[45] Yu.V. Knyazev, D.A. Balaev, S.V. Stolyar, O.A. Bayukov, R.N. Yaroslavtsev, V.P. Ladygina, D.A. Velikanov, R.S. Iskhakov. J. Alloys Comp. **851**, 156753 (2021).

[46] Yu.V. Knyazev, D.A. Balaev, S.V. Stolyar, A.A. Krasikov, O.A. Bayukov, M.N. Volochaev, R.N. Yaroslavtsev, V.P. Ladygina, D.A. Velikanov, R.S. Iskhakov. J. Alloys Comp. **889**, 161623 (2021).

[47] Y.V. Knyazev, D.A. Balaev, V.L. Kirillov, O.A. Bayukov, O.N. Martyanov. Pis'ma ZhETF **108**, 558 (2018).

[48] A.A. Dubrovskiy, D.A. Balaev, K.A. Shaykhutdinov, O.A. Bayukov, O.N. Pletnev, S.S. Yakushkin, G.A. Bukhtiyarova, O.N. Martyanov. J. Appl. Phys. **118**, 213901 (2015).

[49] D.A. Balaev, I.S. Poperechny, A.A. Krasikov, K.A. Shaikhutdinov, A.A. Dubrovskiy, S.I. Popkov, A.D. Balaev, S.S. Yakushkin, G.A. Bukhtiyarova, O.N. Martyanov, Yu.L. Raikher. J. Appl. Phys. **117**, 063908 (2015).

[50] C. Chen, O. Kitakami, Y. Shimada. J. Appl. Phys. **84**, 2184 (1998).

[51] V.P. Shilov, J.-C. Bacri, F. Gazeau, F. Gendron, R. Perzynski, Y.L. Raikher. J. Appl. Phys. **85**, 6642 (1999).

[52] A. Aharoni. J. Appl. Phys. **61**, 3302 (1987).

[53] F. Bødker, S. Mørup, S. Linderoth. Phys. Rev. Lett. **72**, 282 (1994).

[54] R.D. Zysler, M. Vasquez Mansilla, D. Fiorani. Eur. Phys. J. B **41**, 171 (2004).

[55] M.P. Proenca, C.T. Sousa, A.M. Pereira, P.B. Tavares, J. Ventura, M. Vazquez, J.P. Araujo. Phys. Chem. Chem. Phys. **13**, 9561 (2011).

[56] X. Batlle, A. Labarta. J. Phys. D **35**, R15 (2002).

[57] C.-R. Lin, R.-K. Chiang, J.-S. Wang, T.-W. Sung. J. Appl. Phys. **99**, 08N710 (2006).

[58] D.A. Balaev, A.A. Krasikov, S.I. Popkov, A.A. Dubrovskiy, S.V. Semenov, D.A. Velikanov, V.L. Kirillov, O.N. Martyanov. J. Magn. Magn. Mater. **515**, 167307 (2020).

[59] D.A. Balaev, S.V. Semenov, A.A. Dubrovskiy, S.S. Yakushkin, V.L. Kirillov, O.N. Martyanov. J. Magn. Magn. Mater. **440**, 199 (2017).

[60] I.G. Vazhenina, R.S. Iskhakov, L.A. Chekanova. FTT **60**, *2*, 287 (2018). (in Russian).

[61] D.A. Balaev, I.S. Poperechny, A.A. Krasikov, S.V. Semenov, S.I. Popkov, Y.V. Knyazev, V.L. Kirillov, S.S. Yakushkin, O.N. Martyanov, Y.L. Raikher. J. Phys. D **54**, 275003 (2021).

[62] D.A. Balaev, A.A. Krasikov, S.I. Popkov, S.V. Semenov, M.N. Volochaev, D.A. Velikanov, V.L. Kirillov, O.N. Martyanov. J. Magn. Magn. Mater. **539**, 168343 (2021).

[63] D.A. Balaev, A.A. Dubrovsky, S.S. Yakushkin, G.A. Bukhtiyarova, O.N. Martyanov. FTT **61**, 478 (2019). (in Russian).

[64] J.L. Garcıa-Munoz, A. Romaguera, F. Fauth, J. Nogues, M. Gich. Chem. Mater. **29**, 9705 (2017).

[65] R. Jones, R. Nickel, P.K. Manna, J. Hilman, J. van Lierop. Phys. Rev. B **100**, 094425 (2019).

[66] A.A. Dubrovskiy, S.V. Semenov, Yu.V. Knyazev, S.I. Popkov, S.S. Yakushkin, V.L. Kirillov, O.N. Martyanov, D.A. Balaev. IEEE Magn. Lett. **10**, 6110103 (2019).

Translated by Ego Translating